Estimation of Temperature, Microstructure and Deformations in Strip Hardening Industrial Process

Yalçın Kaymak[1], Andreas Heßler[2], Roman Kuziak[3]
1. VDEh-Betriebsforschungsinstitut, Düsseldorf, NRW, Germany
2. HUGO VOGELSANG GmbH & Co. KG, Hagen, NRW, Germany
3. Instytut Metalurgii Zelaza, Gliwice, Poland

Introduction

In automotive and construction markets, the quest for high strength to weight ratio components is continuously increasing. High strength materials have also higher residual stresses and consequently more distortion. Therefore, reducing the rejection level of the heat treated advanced high strength steel (AHSS) strips is an active research area. In this study, the evolution of the residual stress and strip flatness in an industrial hardening line are investigated. In this process, most residual stresses are introduced by the quenching in the lead bath and subsequent leveling rollers where also the martensite microstructure forms. The introduced models compute the stress and deformation due to bainite and martensite transformations as well as thermal shrinkage during cooling. The latent heats, transformation induced plasticity (TRIP), creep, plasticity, geometrical nonlinearity (bending by leveling rollers and post-buckling shape) are considered.

The temperature and the displacement fields are computed using the built-in heat transfer in solids and solid mechanics physics in Comsol Multiphysics®. Other state variables which are stored at integration points such as the transformation incubation indicator, phase fractions, TRIP and creep strains are implemented as distributed ordinary differential equations. The transformation kinetics for bainite formation is assumed to obey the Scheil's additivity rule and Johnson-Mehl-Avrami-Kolmogorow (JMAK) equation. The martensite transformation is described by the Koistinen-Marburger (KM) equation. The TRIP is based upon the Greenwood–Johnson (GJ) mechanism. The material properties of each phase are described by temperature dependent functions and the overall properties are expressed using mixture rules.

The strip is assumed to be stress and deformation free and fully austenite before quenching in the lead bath. Then, it is quenched to almost uniform temperature just above the martensite transformation start temperature. Afterwards, it is cooled down slowly to obtain a martensitic microstructure. During the martensite transformation, the strip is constrained in out of plane direction by a series of leveling rollers. These rollers also bend the strip up and down which introduces controlled bending stresses at the strip cross-section. These stresses are then mostly relaxed and equalized by the development of inelastic strains (including TRIP and creep phenomenon). The sequence of these complex processes is modeled using a series of components and study steps in Comsol Multiphysics®.

The solution strategy is composed of following four study steps:

1) Compute temperature and microstructure of the moving strip (3d component, stationary).
2) Compute bending configuration of the strip in the leveling rollers (2d component, parametric, stationary contact).
3) So-called 2.5d deformation analysis by a generalized plane strain (2d component, transient).
4) 3d nonlinear post-buckling analysis using the stress state from step 3 (3d component, stationary).

The temperature evolution along the strip during the heat treatment process was measured by special in-situ campaigns performed at HUGO VOGELSANG (HUVO). The measured temperatures were used to estimate the heat transfer coefficients in the lead bath. Also, the measured temperature was used in the dilatometry measurements by Instytut Metalurgii Zelaza (IMZ) to get the material Time-Temperature-Transformation (TTT) diagram and creep characteristics. The simulations of the experiments are performed to calibrate and validate the material model.

Theory and Governing Equations

The material model is developed for computing the stress and deformation during the cooling (or quenching) due to bainite and martensite transformations as well as thermal shrinkage. The model considers latent heats, transformation induced plasticity (TRIP), creep, plasticity, geometrical nonlinearity (large deformations). The modelled couplings among the temperature, displacement and phase fields are highlighted in **Figure 1**. The Temperature and phase fields are bidirectionally coupled and, therefore, simultaneously solved in step 1.

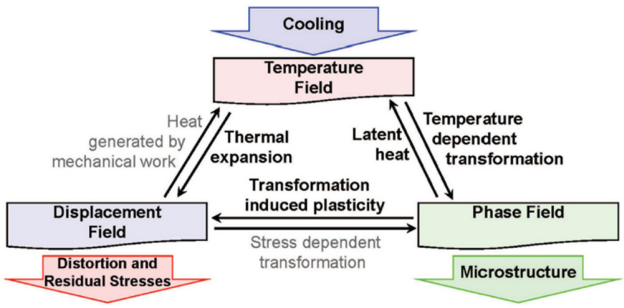

Figure 1. Coupling of fields in quenching process.

The simulation model was developed using the COMSOL Multiphysics® software. The basics of the modelling approach can be found in the PhD thesis [1] and further details about Comsol

implementation can be found in [2]. The temperature field and the displacement field are computed using the built-in heat transfer in solids and solid mechanics physics in the software. State variables (the transformation start indicator, phase fractions, TRIP and creep strains) are implemented as distributed ordinary differential equations and their values are stored at integration points. The transformation kinetics for bainite formation is assumed to obey the Scheil's additivity rule and the JMAK-equation [3-6]. The martensite transformation is described by the KM-equation [7]. The TRIP is based upon the GJ-mechanism [8-9]. Furthermore, the material properties of each phase are described by temperature dependent functions and the overall properties are expresses using mixture rules as given in Equations (1).

$$\left.\begin{aligned} E &= f_a E_a(T) + f_b E_b(T) + f_m E_m(T) \\ \nu &= f_a \nu_a(T) + f_b \nu_b(T) + f_m \nu_m(T) \\ \sigma_{y0} &= f_a \sigma_{ay0}(T) + f_b \sigma_{by0}(T) + f_m \sigma_{my0}(T) \\ C_p &= f_a C_{pa}(T) + f_b C_{pb}(T) + f_m C_{pm}(T) \\ k &= f_a k_a(T) + f_b k_b(T) + f_m k_m(T) \\ \rho &= \frac{1}{\frac{f_a}{\rho_a(T)} + \frac{f_b}{\rho_b(T)} + \frac{f_m}{\rho_m(T)}} \end{aligned}\right\} \quad (1)$$

where T is temperature, f volume fraction, E elasticity module, ν Poisson's ratio, σ_{y0} initial yield stress, C_p heat capacity, k thermal conductivity and ρ density. Subscript a denotes austenite, b bainite and m martensite phases. For the sake of simplicity, a perfectly plastic behavior is assumed. The displacement field is solved using the solid mechanics physics of the software. Inelastic strains due to TRIP and creep are included as initial strains and the dilatation due to the temperature and microstructure changes are added as user defined thermal expansion. The volumetric strain (or dilatation) is given by Equation (2):

$$dV = \sqrt[3]{\frac{\rho_a(T_{ref})}{\rho}} - 1 \quad (2)$$

where T_{ref} is the strain reference temperature, ρ_a the austenite density and ρ the current density.

Sub-model for bainite and martensite transformation: two state variables are defined per integration point, the transformation incubation indicator (Scheil's sum) as ss in Equation (3) and the bainite volume fraction as f_b as in Equation (4). The bainite transformation starts at time $Bs(T)$, which is a function of temperature and taken from the TTT-diagram. The JMAK-factor K and JMAK-exponent n are given in Equation (5) for the volume fraction range [0.01, 0.999]. The state variable ss and f_b are integrated by the solver at each integration (quadrature) point.

$$\dot{ss} = \frac{1}{Bs(T)} \quad (3)$$

$$\dot{fb} = K \cdot n \cdot t^{n-1} \cdot \exp(-K \cdot t^n) \quad \text{if} \quad ss > 1 \quad (4)$$

$$n = \frac{-\ln\left(\frac{\ln(1-0.01)}{\ln(1-0.999)}\right)}{\ln(Bf(T)) - \ln(\ln(10))} \cdot \quad \text{and} \quad K = \frac{\ln(1-0.01)}{n \cdot \ln(Bs(T))} \quad (5)$$

The martensite transformation of the retained austenite fraction is simply implemented by the KM-equation, which does not require any additional PDEs to solve or integrate. It is assumed that martensite forms below the martensite start temperature M_s and the martensite volume fraction f_m only depends on the temperature T as given in Equation (6).

$$f_m = (1 - f_b)\{1 - \exp(-0.011(M_s - T))\} \quad (6)$$

Sub-model for TRIP and creep: the components of the symmetric inelastic strain tensor are defined as state variables per integration point, namely ec_{ij} (i,j=1,2,3) as given in Equation (7). Additionally, an effective inelastic strain, ec_{eff} is also defined as given in Equation (8) and stored. Thus, 7 state variables ($ec_{11}, ec_{22}, ec_{33}, ec_{12}, ec_{13}, ec_{23}, ec_{eff}$) are defined and stored per integration point. The inelastic deformation increment occurs in the unit direction of stress deviator, n_{ij}^S. A_{tr} defines the transformation TRIP part of the inelastic strain rate and A_{cr} defines the creep part. The expression for A_{tr} is given in Equation (9), where K_m^{GJ} and K_b^{GJ} are transformation plasticity constants due to the GJ-mechanism for martensite and for bainite, the f_m and f_b represent the volume fraction of martensite and bainite, respectively. The expression for A_{cr} is given in Equation (10), which is simply the Norton's creep law with temperature dependent σ_{ref} and exponent n_{cr}. The reference stress σ_{ref} and exponent n_{cr} are experimentaly determined material properties.

$$\dot{ec}_{ij} = (A_{tr} + A_{cr}) \cdot n_{ij}^S \quad (7)$$

$$\dot{ec}_{eff} = \sqrt{\frac{2}{3}\sum \dot{ec}_{ij}^2} \quad (8)$$

$$A_{tr} = \left\{K_m^{GJ} \cdot \dot{f}_m \cdot \ln(f_m) + K_b^{GJ} \cdot \dot{f}_b \cdot \ln(f_b)\right\} \cdot \sigma_{eff} \quad \text{if} \quad f_m,\, f_b > 0.03 \quad (9)$$

$$A_{cr} = \left(\frac{\sigma_{eff}}{\sigma_{ref}}\right)^{n_{cr}} \quad (10)$$

Temperature field model: the temperature field is solved by the heat transfer in solids physics in Comsol Multiphysics®. The temperature field in solid material is modelled by Fourier's heat conduction Equation (11). Temperature field is bi-directionally coupled to the microstructure field, so they are solved simultaneously.

$$\begin{aligned} &\rho \cdot C_p \frac{\partial T}{\partial t} + \nabla \cdot \mathbf{q} = Q \\ &\mathbf{q} = -k \nabla T \end{aligned} \quad (11)$$

where, ρ is the density, C_p the heat capacity, T temperature field, t the time, $\mathbf{q}$ heat flux vector, k thermal conductivity and Q heat source due to the latent heat of the phase transformations. The equation for the heat source Q depends on the transformation latent heats as well as the phase transformation rates. It is defined by the Equation (12) in the model:

$$Q = L_{ab}\dot{f}_b + L_{am}\dot{f}_m \quad (12)$$

where, L_{ab} and L_{am} are the latent heats of the austenite to bainite and austenite to martensite transformations, $\dot{f}_b$ and $\dot{f}_m$ are

the rates of the austenite to bainite and austenite to martensite transformations, respectively.

Model Calibration by Measurements

The temperature evolution along the strip during the strip hardening industrial process is measured by special in-situ experiments. The thermocouples are fixed on the strip by welding. Also, a thin protection cover is welded above the thermocouple front as shown in **Figure 2** so that they stay attached along the process line. The measured temperature evolution is used to estimate the cooling heat transfer coefficients at the lead bath. Also, the measured temperature evolution is used in the dilatometry measurements by IMZ to get material TTT-diagram or creep characteristics. The simulations of the experiments are performed to calibrate and validate the material model.

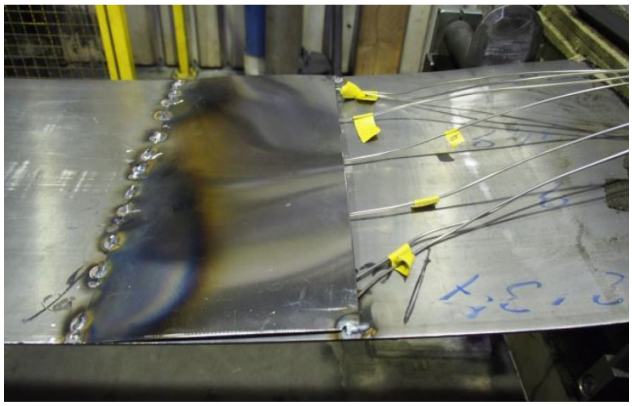

Figure 2. In-situ measurement of temperature evolution and attachment of thermocouples to the strip.

A series of dilatometry measurements is performed in order to identify the material properties. The typical geometry of the dilatometry specimen is shown **Figure 3**. The specimen is fixed in the dilatometry device using the two holes at its ends. The region of interest is the narrow middle region of the specimen. The dilatometry device is programed to apply a given temperature and mechanical loading sequence. The specimen temperature T is continuously monitored using a contact thermocouple as well as the elongation of ΔL between the notches of the specimen. The initial distance $\Delta L_0 = 10\text{mm}$. Some of the experimental results are used to calibrate and validate the developed model.

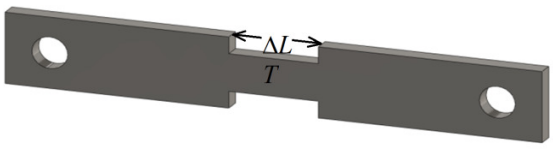

Figure 3. Typical dilatometry specimen geometry.

For phase transformation model calibration and validation, the test specimen is first rapidly cooled from approximately 850°C to 300°C and then kept at that temperature under 20MPa tensile load for approximately 2000s until the bainite transformation is completed meanwhile the elongation of narrow section between the notches ($d\Delta L$) of the specimen is recorded. The model geometry with mesh is shown in **Figure 4**. Due to symmetries only one eighth of the geometry is modelled and the holes are skipped for the simplicity. The measured (blue curve) and computed (green curve with circle markers) elongations of narrow section between the notches ($d\Delta L$) are compared in **Figure 5**. Note that the simulation does not includes the heating and austenisation, but it starts at time tcs (time of cooling start).

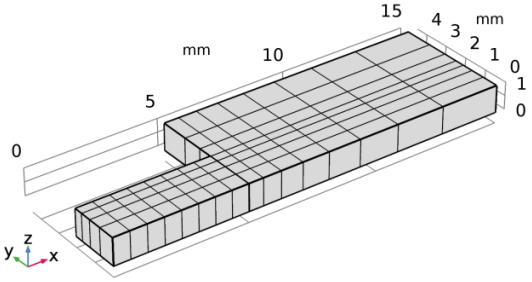

Figure 4. Model geometry and mesh of the specimen

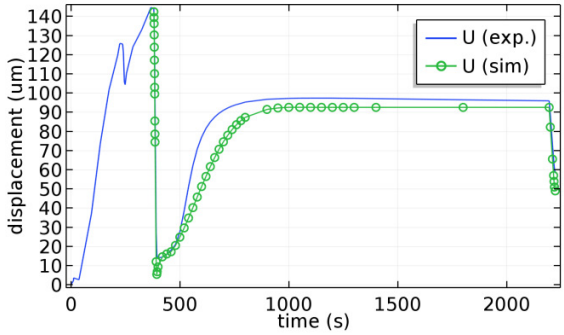

Figure 5. Specimen elongation ($d\Delta L$) TRIP test.

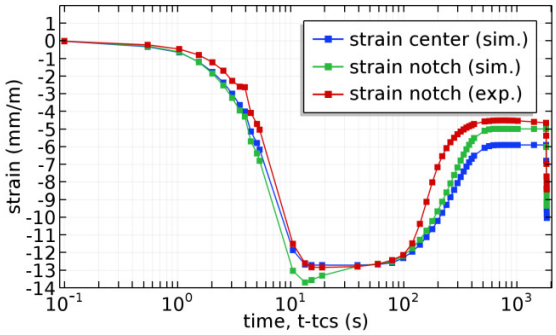

Figure 6. Strain history in TRIP test.

An average engineering strain can be estimated by $d\Delta L/\Delta L_0$ from the elongation measurement (which corresponds to red curve in **Figure 6**). In the numerical model, the average axial strain at middle section (which corresponds to blue curve in **Figure 6**) and model estimated engineering axial strain (which corresponds to green curve in **Figure 6**) are both computed for comparison. Although a simple phase transformation model is chosen and the exact placement of the strain gauge arms at the notches is not considered in the model evaluation, the model results are consistent with the dilatometry tests and satisfactorily good for the intended usage.

The thermal shrinkage during the cooling, and the elongation due to the phase transformation dilatation can be better distinguished in the temperature-strain relation as shown in **Figure 7**. The vertical jump is due to the dilatation during the austenite to

bainite isothermal phase transformation. The linear parts represent the thermal shrinkages of austenite at higher temperatures and of bainite at lower temperatures.

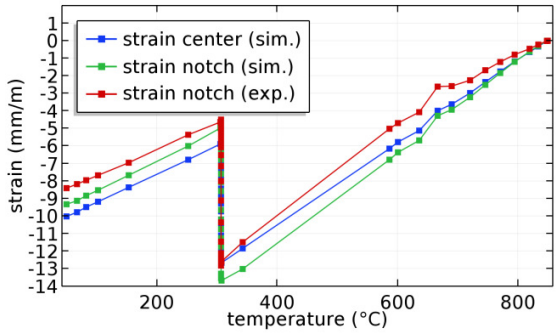

Figure 7. Strain-temperature relation (dilatometry) in TRIP test.

The evolutions of the Scheil's sum ss and the microstructures are shown in **Figure 8**. The volume average of the Scheil's sum ss is the blue curve with stars, when it reaches the unity, then it means the incubation time is complete and the austenite to bainite transformation starts. The state variable Scheil's sum is meaningful only until it reaches to unity. So, a cut-off after 1.2 is applied for large values. The volume average of the bainite volume fraction f_b is plotted by the green curve with circles. As the bainite forms, the austenite (f_a the turquoise curve with squares) is equally consumed. Only the bainite transformation was targeted in the experiment. There is no martensite (f_m red curve with diamonds) formation.

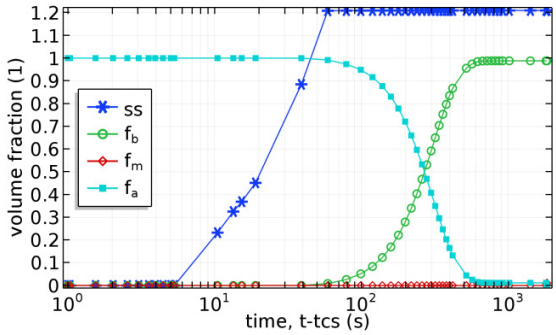

Figure 8. Evolutions of the Scheil's sum and the microstructures.

The phase transformation related data (TTT-diagram and cooling curves) is summarized in **Figure 9**. The solid curves without markers are ferrite start (FsRef), pearlite start (PsRef), pearlite finish (PfRef), bainite start (BsRef) and bainite finish curves (BfRef), respectively. These curves are just shown as info for referencing the literature curves. The curves with markers are used in the simulation model as input. The green curve with squares and red curve with pluses are bainite start (Bs) and finish (Bf) curves, respectively. The black curve with circles and blue curve with diamonds are martensite start (Ms) and martensite finish (Mf) temperatures, respectively. The yellow curve with stars is the volume averaged temperature (Tav) over the region of interest (narrow middle region of the specimen).

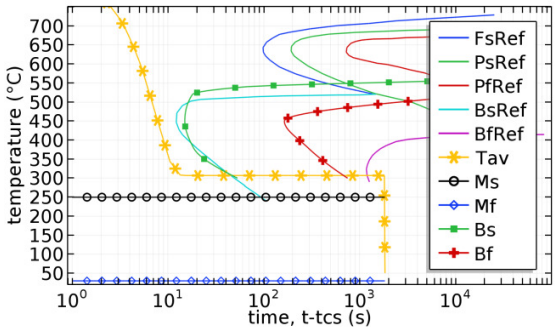

Figure 9. TTT diagram and cooling curve.

For creep model calibration and validation, the test specimen kept at 750°C, under 80MPa tensile stress for approximately 5000s, until its creep failure. The same model geometry and mesh as shown in **Figure 4** is used. To achieve the tensile stress, a constant load is applied during the experiment. So, the true tensile stress increases as the cross-sectional area is contracted as shown in **Figure 10**.. Ultimately, the specimen ruptures at the middle. Again, the elongation of narrow section between the notches ($d\Delta L$) of the specimen is recorded.

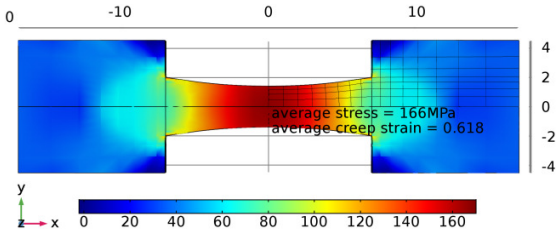

Figure 10. Stress field just before creep failure.

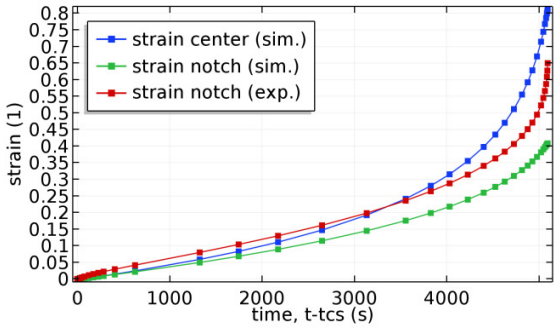

Figure 11. Strain history in creep test.

An average engineering strain can be estimated by $d\Delta L/\Delta L_0$ from the elongation measurement (which corresponds to red curve in **Figure 11**). In the numerical model, the average axial strain at middle section (which corresponds to blue curve in **Figure 11**) and model estimated engineering axial strain (which corresponds to green curve in **Figure 11**) are both computed for comparison. Since the Norton's creep law is the simplest among the creep laws, it is capability to describe the complete creep evolution is limited. Besides, the exact placement of the strain gauge arms at the notches is not considered in the model evaluation. Nevertheless, the model results are consistent with the dilatometry tests and satisfactorily good for the intended usage.

Simulation Methods and Discussion of the Results

In the industrial strip hardening process, the strip is austenitized by heating and desired microstructure is achieved by controlled cooling. In the current model, the strip is assumed to be stress and deformation free and fully austenite before quenching in lead bath. The strip is quenched in the lead bath to almost uniform temperature just above the martensite transformation start temperature M_s. Afterwards, it is cooled down slowly by a series of air nozzles to obtain a martensitic microstructure. Meanwhile, the strip is constrained in out of plane direction by a series of leveling rollers as it moves in between the air nozzles. These leveling rollers also bend the strip up and down to control strip flatness. This produces a light increase in the overall tensile stress and introduces controlled bending stresses. These stresses are then mostly relaxed and equalized as the inelastic strains developed by TRIP and creep phenomenon.

During the strip hardening process, small temperature gradients along the width combined with the phase transformations can lead to high compressive stresses and local elastic buckling. The compression stresses and the out of plane deformation upon buckling can be possibly avoided by the correct configuration of the leveling rollers. The aim of the model is to compute the influences of the leveling rollers.

An example of typical buckling and out-of-plane deformation calculation procedure is given to explain the adopted solution strategy. The typical geometry and the thermal boundary conditions during the quenching sub-process are schematically shown in **Figure 12**. The strip thickness is bh = 2.24mm, width is bw = 310mm, band speed is vb = 2.8m/min, material is 50CrMo4.

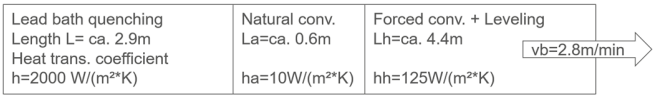

Figure 12. Typical thermal boundary conditions of the strip.

The sequence of the complex processes is modeled using a series of components and study steps in Comsol Multiphysics®. The solution strategy is composed of following four steps:

1) Compute temperature and microstructure of the moving strip (3d component, stationary).
2) Compute bending configuration of the strip in the leveling rollers (2d component, parametric, stationary contact).
3) So-called 2.5d deformation analysis by a generalized plane strain (2d component, transient).
4) 3d nonlinear post-buckling analysis using the stress state from step 3 (3d component, stationary).

In step 1, the steady state temperature and microstructure fields are computed in the symmetric half of the strip. The equations involving time derivatives should be modified by using the chain derivative rule so that they are expressed in terms of strip speed vb (e.g., $\dot{ss} = vb \cdot \partial ss/\partial y$ if the strip is moving in y-direction). That means the distributed PDE for the Scheil's sum as $\dot{ss}$ in Equation (3), the bainite volume fraction as $\dot{f}_b$ as in Equation (4), and the latent heat source term in the Equation (12), should be modified accordingly. A structured mesh is used with 120.000 hexahedral elements. The mesh grid contains 6 elements in thickness direction, 20 elements in the width direction and 1000 elements in the strip axial direction. The solved values of temperature and microstructure from step 1 can be retrieved later in 2d transient analysis in step 3 with the help of general extrusion operator by defining the destination map as [X, vb*t, Z].

The temperature evolution is shown over the measured TTT-diagram of the material in **Figure 13**. The red curve with diamonds shows the segment of the special in-situ temperature measurement Tm. The turquoise solid line shows the computed temperature evolution T at x=0, z=-bh/2. This position also roughly corresponds to the measurement points. The purple solid line shows the computed temperature evolution T at x=bw/2, z=-bh/2. Note that the corner cools faster than the center when the strip initially submerged in the lead bath, but they have almost the same temperature when they leave the bath. The bainite start Bs and finish Bf curves are indeed experimentally measured and are shown by blue solid curve with asterisk markers and green solid curve with circle markers, respectively.

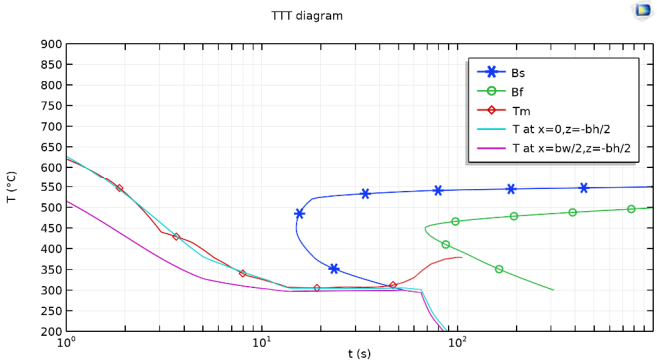

Figure 13. Temperature evolution during the quenching plotted on TTT-diagram of the material.

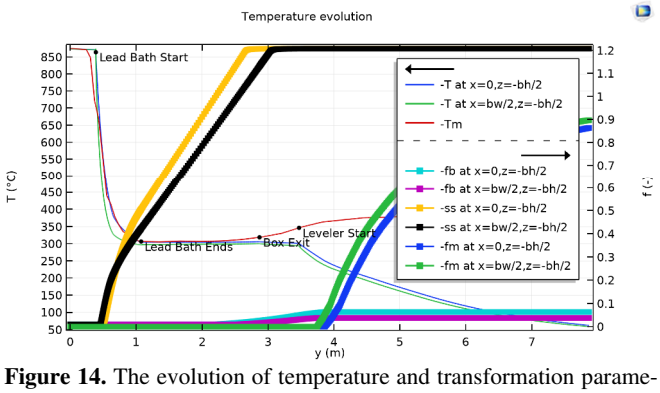

Figure 14. The evolution of temperature and transformation parameters during the quenching.

Further results related to phase transformations are given in **Figure 14** with a temperature axis on the left y-axis and microstructure axis on the right y-axis. The position along the strip is represented by the x-axis. The solid red curve shows the segment of the special in-situ temperature measurement Tm. The secondary air cooling for martensite formation was not meas-

ured because it was not possible to drive the thermocouple attached strip through the leveling rollers. So, the part of the solid red curve after Leveler Start is not relevant. The solid blue and solid green curves show the temperature computed by the simulation model along the strip center (T at x=0, z=-bh/2) and edge (T at x=bw/2, z=-bh/2), respectively. The yellow and black curves with square markers show the Scheil's sum along the strip center (ss at x=0, z=-bh/2) and edge (ss at x=bw/2, z=-bh/2), respectively. The Scheil's sum indicates the completion of incubation time for the bainite transformation start. The turquoise and purple curves with square markers show the computed bainite volume fraction along the strip center (fb at x=0, z=-bh/2) and edge (fb at x=bw/2, z=-bh/2), respectively. The blue and green curves with square markers show the computed martensite volume fraction along the strip center (fm at x=0, z=-bh/2) and edge (fm at x=bw/2, z=-bh/2), respectively. The slight time shift of phase transformation between the central part and edge part ultimately produces a characteristic stress distribution through the width of the strip. If the stresses are high, this may even lead to the buckling of the strip.

In step 2, the stationary bending behavior of the strip in the leveling rollers is separately calculated as a contact problem with a parametric solver. The rigid leveling rollers above and below the strip are shown in **Figure 15**. The lower rollers have fixed positions whereas the upper rollers packed in 4 cassettes each of which holds 4 pieces of rollers. These cassettes can be moved up and down to control the penetration depths and the levelling degree. The configurations of the cassettes, i.e., the displacements (Y1, ..., Y8) are applied to upper rollers, the lower rollers are fixed. The elasto-plastic deformation of the strip is computed using a parametric 2d contact analysis. The computed curvature (vxx) is exported as a text file and it will be an input to the 2D transient analysis of the strip cross-section analysis in step 3. The curvature variation along the strip is shown in **Figure 16**. Note that the sharp curvature peaks for cassete-1 (RR1) indicate plastic bending due to high penetration depth.

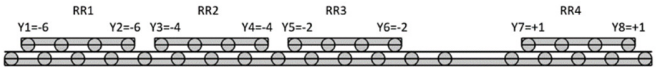

Figure 15. The level rollers at the air-cooling area.

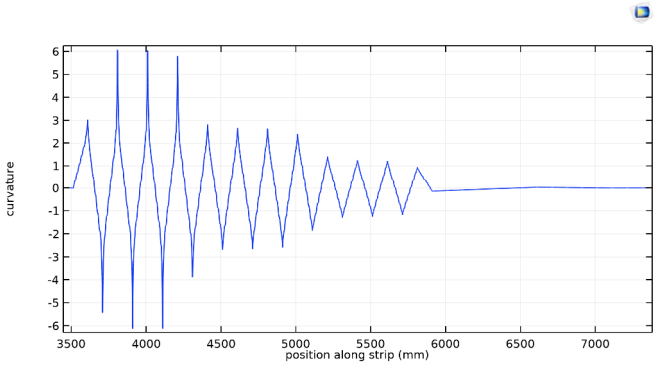

Figure 16. Curvature along the strip which is a measure of strip bending.

In step 3, a transient so-called 2.5d deformation analysis (a generalized plane strain analysis) is performed. The additional half dimension comes from the out-of-plane degrees-of-freedoms (dofs). The out-of-plane strain is computed from a global equation as given in **Table 1** using the known axial strip tension. Then, the out-of-plane strain component WZ is defined in terms of axial stain and bending curvatures. Corresponding default domain equations are manually edited as given in **Table 2**. Note that the bending curvature is defined by the interpolation function KX which was exported as the text file in step 2. The computed temperature and phase fields from step 1 are invoked using the extrusion coupling operator as given in **Table 3**.

Table 1. Use of global equation to compute axial strain.

Name	f(u,ut,utt,t) (Pa)	Initial value (u_0) (1)	Initial value (u_t0)	Description
DZ	SZapp(vb*t)-aveop1(solid.sz)	0	0	axial strain. (beam dof)

Table 2. Modification of default domain equations to consider the axial strain and curvature.

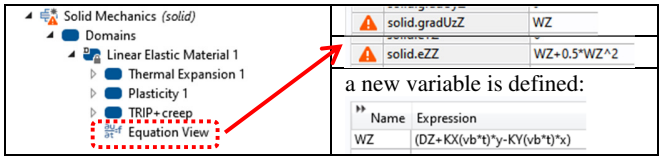

Table 3. Use of extrusion operator to recall solution from step 1.

Name	Expression	Unit	Description
fa	comp1.genext1(comp1.fa)		comp2.fa
fm	comp1.genext1(comp1.fm)		comp2.fm
fb	comp1.genext1(comp1.fb)		comp2.fb
T	comp1.genext1(comp1.T)	K	comp2.T
fmt	comp1.genext1(comp1.fmy)*vb	1/s	comp2.fmt
fbt	comp1.genext1(comp1.fby)*vb	1/s	comp2.fbt

The linear elastic material model is extended to include the thermal expansion, plastic strains as well as TRIP and creep strains. The TRIP and creep strains (given in Equation (7)) are integrated at gauss points using distributed PDE. After solving step 3, the stress, strain and displacement components needed to be mapped to a 3d domain from this time dependent solution. So, a new Parametric Extrusion solution set is generated where the extrusion maps the time to the axial strip position. From this extrusion data set, the necessary stress, strain and displacement components are exported as text files. They will be later re-imported in step 4 to compute the post-buckling analysis.

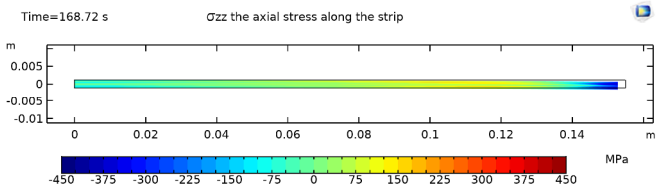

Figure 17. Model geometry and boundary conditions for the buckling deformation during quenching.

The computed longitudinal stress component σzz over the symmetric half cross-section of the strip (x=0 is symmetry axis) is shown in **Figure 17**. The red color means tension and blue color means compression. The edge of the strip undergoes high compression which may lead to edge buckling. The evolution of axial stress is further discussed in **Figure 18**, where the solid blue and solid green curves show the longitudinal stress σzz along the strip center (szz at x=0, z=0) and edge (szz at x=bw/2,

z=bh/2), respectively. The zig-zag patterns are due to the leveling rollers, which bend the strip repeatedly up and down. After the leveling rollers, high residual compressive stress remains at the edges.

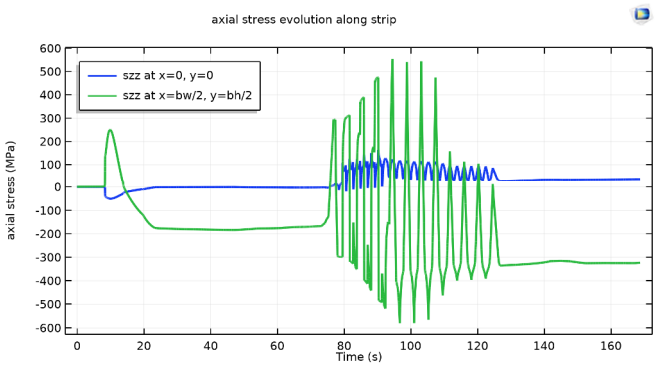

Figure 18. Blue and green line show the stresses along center and edge of the strip.

Finally, in step 4, a 3d nonlinear post-buckling analysis of full 3d strip is carried out. The stress, strain and displacement results of the 2.5D from step 3 can be re-imported as interpolation functions. Initial (residual) stress are defined using these interpolation functions. The initial longitudinal stress SY is shown in **Figure 19** for the bottom and top faces of the strip during the process.

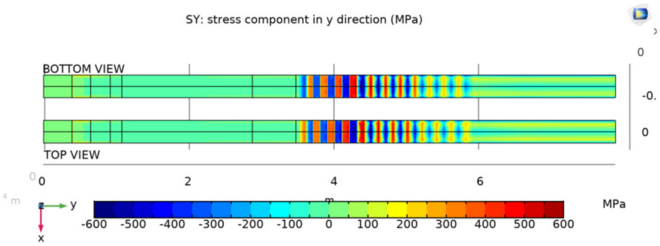

Figure 19. The axial stress distribution at the bottom and top surfaces of the strip during the process.

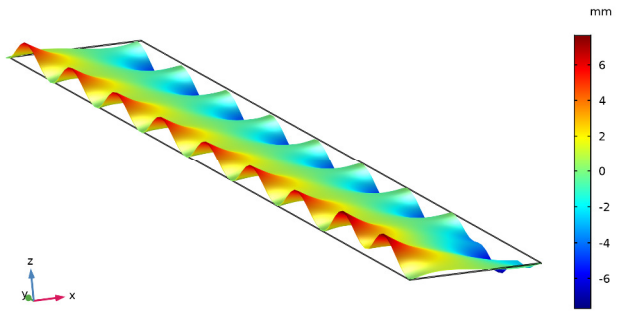

Figure 20. Post buckling shape of the strip for the 1.75 times scaled internal stress state at the end of leveling rollers when 8 MPa tension applied (the deformations are magnified by factor 10).

For the post buckling shape of the strip, a strip segment of 4m length is modeled. The initial stresses are set from the last time step result of the 2.5D from step 3. The straightening effect of the pre-applied tensile stress is included with the help of an additional global equation. The geometrical nonlinearities are included for the solution. For this specific case, there was no edge buckling. So, the initial stresses are scaled with factor 1.75 to demonstrate the model capability to compute the strip buckling shape which is shown in **Figure 20**. The deformations are magnified 10 times to make the buckling shape visible. The model estimates about 7mm edge waviness. The actual process chain has also flattening press furnace and tempering furnace to reduce these high residual stress.

Conclusions and Summary

A mathematical model for the modeling of metal heat treatment process is introduced at the beginning of this paper. Then, the model is calibrated and validated by the measurements at the industrial plant and laboratory. Finally, this model is applied to estimate the temperature, microstructure and deformation in a typical strip hardening industrial process using a series of study steps in Comsol Multiphysics®.

References

1. Y. Kaymak, Simulation of Metal Quenching Process for the Minimization of Distortion and stresses, PhD thesis, Otto-von-Guericke Universität (2007).
2. Y. Kaymak, Phase Transformation and Deformation Model for Quenching Simulations, Comsol Conf., Rotterdam (2017).
3. M. Avrami, Kinetics of phase change 1 - general theory. J. Chem. Phys., 7:1103-1112 (1939)
4. M. Avrami, Kinetics of phase change 2 - transformation-time relations random distribution of nuclei. J. Chem. Phys., 8:212-224 (1940)
5. M. Avrami, Kinetics of phase change 3 - granulation, phase change and microstucture. J. Chem. Phys., 9:177-184 (1941)
6. Cemil Hakan Gur, Jiansheng Pan, Handbook of thermal process modelling of steels. CRC Press (2009)
7. D. Ivanov, L. Markegard, Stress relaxation by trans-formation plasticity under the martensitic transformation in steels. HTM J. Heat Treatm. Mat. 71 (2016)
8. T. Otsuka, T. Akashi, S. Ogawa, T. Imai, A. Egami, Effect of volume expansion on transformation plasticity during ferrite and martensite transformation of steels; Journal of the society of materials science, Japan, Vol. 60, No.10, pp. 937-942 (2011)
9. E. Anderson Ariza, et.al., Numerical simulation with thorough experimental validation to predict the build-up of residual stresses during quenching of carbon and low-alloy steels; ISIJ International, Vol. 54, No. 6, pp. 1396-1405 (2014)

Acknowledgements

The work presented here has been carried out with a financial grant from the Research Fund for Coal and Steel (RFCS) of the European Community with Grant Agreement No: RFSR-CT-2015-00012 and project title "*Optimal Residual Stress Control*" (ORSC).